1958 (Pergamon, New York, 1960), pp. 148–161.
19. H. B. Zimmerman, *Geol. Soc. Am. Bull.* **83**, 3709 (1972).
20. J. Neiheisel and C. E. Weaver, *J. Sediment. Petrol.* **37**, 1084 (1967).
21. D. R. Pevear, *Geol. Soc. Am. Mem. 133* (1972), p. 317.
22. J. W. Pierce, *Southeast. Geol.* **12**, 33 (1970).
23. C. E. Weaver, *Geochem. Cosmochim. Acta* **31**, 2181 (1967).
24. V. E. McKelvey, *Ocean Manage.* **1**, 119 (March 1973).
25. Massachusetts Institute of Technology, "Oil spill trajectory studies for Atlantic Coast and Gulf of Alaska," in *Primary, Physical Impacts of Offshore Petroleum Development*, prepared for the Council on Environmental Quality under contract No. EQC 330 (Massachusetts Institute of Technology, Cambridge, Mass., 1974), Report No. MIT SG 74-20.
26. M. Cashman, "Tankers will be safer in the future," *Ocean Industry* (March 1975), pp. 44–46.
27. A. E. Gibson, *Energy and Public Policy—1972* (The Conference Board, Inc., New York, 1972), pp. 188–192.
28. R. E. Lapp, "Adding things up, big doesn't mean efficient," *New Republic* (20 November 1971), pp. 25–27.
29. D. Livingston, *Environment* **16**, 38 (September 1974).
30. O. Schachter and D. Serwer, *Am. J. Int. Law* **65** (No. 1) (January 1971).
31. S. Berman, *J. Maritime Law Comm.* **5**, 1 (1973).
32. S. S. Kalsi, *Environ. Aff.* **3** (No. 1), 79 (1974).
33. R. Wilson and W. J. Jones, *Energy, Ecology, and the Environment* (Academic Press, New York, 1974), p. 301.
34. F. R. Kesterman and K. G. Hay, *J. Maritime Law Comm.* **5**, 708 (July 1974).
35. Massachusetts Institute of Technology, "Oil spill trajectory studies for Atlantic Coast and Gulf of Alaska," in *Primary, Physical Impacts of Offshore Petroleum Developments*, prepared for the Council on Environmental Quality under contract No. EQC 330 (Massachusetts Institute of Technology, Cambridge, Mass., 1974), Report No. MIT SG 74-20.
36. University of Oklahoma Technology Assessment Group, *Energy Under the Oceans: A Technology Assessment of Outer Continental Shelf Oil and Gas Operations* (University of Oklahoma Press, Norman, 1973), with U.S. Geological Survey, U.S. Coast Guard, and Oil and Gas Journal data.
37. D. Charter and J. Porricelli, paper presented at the May 1973 Workshop on Inputs, Fates and Effects of Petroleum in the Marine Environment (National Academy of Sciences–National Research Council, Washington, D.C., 1973); R. Osgood, A. Hollick, C. Pearson, J. Orr, *Toward a National Ocean Policy: 1976 and Beyond* (Government Printing Office, Washington, D.C., 1976); R. Revelle, E. Wenk, B. Ketchum, E. Corino, "Ocean pollution by petroleum hydrocarbons," *Man's Impact on Terrestrial and Oceanic Ecosystems* (MIT Press, Cambridge, Mass., 1971).
38. We thank H. D. Hedberg, C. A. Burk, and P. A. Parsons for valuable criticism and suggestions.

Structural Domains of Transfer RNA Molecules

The ribose 2′ hydroxyl which distinguishes RNA from DNA plays a key role in stabilizing tRNA structure.

Gary J. Quigley and Alexander Rich

DNA and RNA are the major macromolecules used for the transfer of information in biological systems. They differ from each other principally by the presence of a hydroxyl group on the 2′ position of the ribose sugar in RNA. This systematic difference in the polynucleotide backbone is likely to be related to significant structural and functional differences. DNA is used solely as an information carrier; certain kinds of RNA are also used in this role, including viral RNA and messenger RNA. However, other classes of RNA such as ribosomal and transfer RNA seem to play a significant structural role as well. Ribosomal RNA is believed to form a three-dimensional lattice on which ribosomal proteins are placed in the assembly of the functioning organelle. In the transfer RNA molecule, only the three anticodon nucleotides play a direct role in the transfer of genetic information through their interaction with the three nucleotides in the codon of messenger RNA. Nonetheless, transfer RNA molecules have 74 to 91 nucleotides (*1, 2*). The vast bulk of these are involved in forming a complex three-dimensional structure whose functional role is only partly understood at the present time. For several years, we have been studying the three-dimensional structure of yeast phenylalanine transfer RNA ($tRNA^{Phe}$). This work has led to an understanding of the three-dimensional conformation of this molecule and to some understanding of the three-dimensional structures of tRNA molecules as a class (*3*).

In this article, we review aspects of the three-dimensional structure of yeast $tRNA^{Phe}$ and, in particular, discuss some of the more recent structural findings, which are based on a refinement of the molecular structure. This has led to the recognition that this tRNA molecule has several domains which essentially repeat certain structural features or motifs. In a striking fashion, the refinement has revealed the critical role played by the ribose 2′ hydroxyl group in stabilizing important features of the folding of the RNA polynucleotide chain in the nonhelical regions of the molecule. This has provided us with some perspective on the manner in which nature has utilized RNA molecules to form complex three-dimensional structures. It is likely that some of these features will be seen in the future as we come to understand the three-dimensional structure of other types of RNA, including ribosomal RNA.

Transfer RNA plays a central role in protein synthesis. An amino acid is attached enzymatically to the 3′ end of the molecule, which then enters the ribosome and forms a specific interaction with a codon base triplet of messenger RNA. The growing polypeptide chain is transferred to the amino acid, and the complex of messenger RNA, tRNA, and polypeptide chain is moved to an adjacent site in the ribosome. The polypeptide chain is then transferred to the amino acid attached to a subsequent tRNA which has entered the ribosome, and the original tRNA is released from the ribosome. We would like to understand the molecular basis of these key events in the expression of genetic information.

In 1965, Holley *et al.* (*4*) sequenced the first tRNA and noted that it could be folded into a cloverleaf arrangement in which the stem regions contained complementary bases. Since then, the sequences of some 75 different tRNA molecules have been determined (*1, 2*) and all of them can be organized into this same general cloverleaf folding, which is illustrated for yeast $tRNA^{Phe}$ in Fig. 1a (*5*). From these results has come an awareness that a large number of the positions in the cloverleaf sequence are occupied by constant or invariant nucleotides (en-

Dr. Quigley is a research associate and Dr. Rich is William Thompson Sedgwick professor of biophysics in the Department of Biology, Massachusetts Institute of Technology, Cambridge 02139.

closed in a solid square in Fig. 1a). Other positions are semi-invariant, occupied exclusively by purines or by pyrimidines (shown by the dashed squares in Fig. 1a). The stem and loop regions are named as indicated in Fig. 1a; the anticodon bases (numbered 34 to 36) interact with messenger RNA during protein synthesis. During aminoacylation, an amino acid is esterified onto the 3′ terminal ribose of adenosine 76, which is at the end of the acceptor stem.

The constant features associated with all tRNA molecules include the seven base pairs in the acceptor stem, three or four base pairs in the D stem, and five base pairs and a seven-residue loop in both the anticodon and TψC arms. Eighty percent of tRNA's have either four or five nucleotides in the variable loop, while the remainder have very large loops containing 13 to 21 nucleotides (*1, 2*). In addition, two regions in the D loop have variable numbers of nucleotides. These are labeled α and β in Fig. 1a and flank the two constant guanosine residues in the D loop. These each contain from one to three nucleotides in different tRNA species.

Polynucleotide Chain Folding

Very little was known about the three-dimensional conformation of tRNA, but the discovery in 1968 (*6*) that it was possible to crystallize tRNA molecules made it apparent that the structure would eventually be elucidated. The difficulty in obtaining crystals of sufficient quality and resolution to give a clear picture of the polynucleotide chain slowed the solution of the structure. However, in 1971 it was discovered that the addition of spermine to yeast $tRNA^{Phe}$ would produce orthorhombic crystals of that tRNA which had x-ray diffraction patterns with a resolution close to 2 Å (*7*). Spermine-stabilized yeast $tRNA^{Phe}$ was subsequently found to form well-ordered monoclinic crystals as well (*8*). The folding of the polynucleotide chain in this tRNA was discovered in 1973 through an analysis at 4 Å resolution of the orthorhombic crystals (*9*). An unusual structure emerged from this study. The molecule has a bent or L-shaped appearance in which the acceptor and TψC stems form one leg of the L; the D stem and anticodon stem form the other leg, as shown in Fig. 1b. In this conformation, the anticodon is about 75 Å away from the amino acid acceptor end. Further details of the three-dimensional folding of the molecule were revealed in subsequent studies at 3 Å resolution of the orthorhombic (*10*) and monoclinic (*11*) crystal forms. A number of tertiary interactions were revealed involving base-base hydrogen bonding. The yeast $tRNA^{Phe}$ molecules appeared very similar in these two different lattices, although some significant differences remained. However, on further interpretation of the monoclinic crystal structure at 2.5 Å resolution (*12*), the differences were found to be much fewer than had been suggested from the initial interpretation. At the present time the principal difference in the conformation of the molecule in these two lattices involves the position of the 3′ terminal residue A76. Two independent preliminary refinement analyses have been carried out on the orthorhombic data (*13, 14*), giving rise to two closely related sets of coordinates. Similarly, two sets of preliminary coordinates have been published from the analysis of the monoclinic crystal (*15, 16*). A comparison of three preliminary sets of coordinates has recently been published (*17*).

A significant feature of the tertiary interactions was that they involved many of the nucleotide positions which are invariant or semi-invariant as shown in Fig. 1. Analysis of the structure suggested that the polynucleotide folding of yeast $tRNA^{Phe}$ was a good model for understanding the three-dimensional folding of all tRNA's since the structure could accommodate the nucleotide variations in different tRNA sequences (*3*). Furthermore, it became apparent that this structure could account for the physical and chemical properties in solution of not only $tRNA^{Phe}$ but other tRNA's as well (*1*).

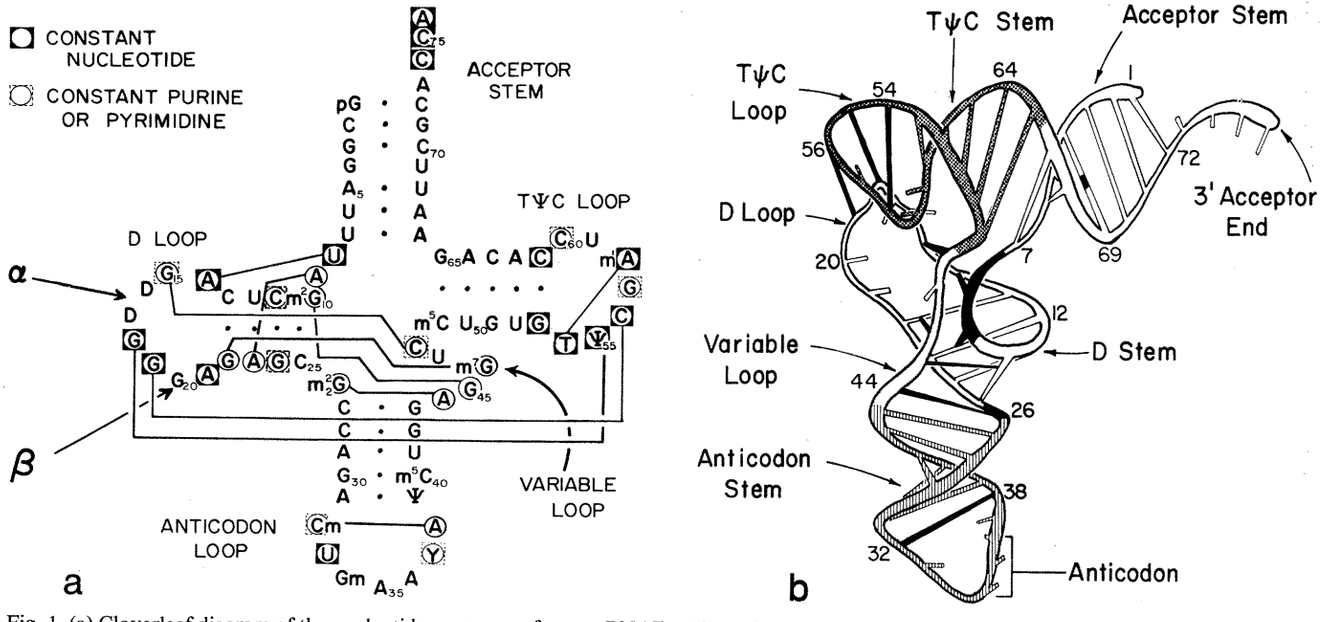

Fig. 1. (a) Cloverleaf diagram of the nucleotide sequence of yeast $tRNA^{Phe}$. The solid lines connecting circled nucleotides indicate tertiary hydrogen bonding between bases. Solid squares around nucleotides indicate that they are constant; dashed squares indicate that they are always purines or pyrimidines. The regions α and β in the D loop contain one to three nucleotides in different tRNA sequences. (b) The folding of the ribose phosphate backbone of yeast $tRNA^{Phe}$ is shown as a coiled tube; the numbers refer to nucleotide residues in the sequence. Hydrogen-bonding interactions between bases are shown as cross rungs. Tertiary interactions between bases are solid black. Bases that are not involved in hydrogen bonding to other bases are shown as shortened rods attached to the backbone.

Molecular Refinement

Recently we have carried out a refinement at 2.5 Å resolution of the molecular coordinates of yeast $tRNA^{Phe}$ in the orthorhombic lattice. In the refinement we used a version of the real-space refinement program of Diamond (*18*), modified to accommodate polynucleotides rather than polypeptides. It was applied in a manner similar to that used by Huber *et al.* (*19*). In these procedures, the approximately 5000 positional degrees of freedom (3 for each of 1700 atoms) are reduced to 500 degrees of freedom. This is done by fixing bond distances and angles of the ribose, phosphate, and base residues to those determined very accurately from structures of small molecules. Positional adjustments are made by shifting the variable dihedral angles of the molecule to change the conformation. Within these constraints, the molecular model is altered to optimize its fit to the electron density map of the structure as calculated from the observed diffraction data and model phase information. The improved model produces improved phase information, which is applied to the observed diffraction data to produce an improved map. This procedure is iterated, and, as the map and model improve, solvent molecules and ions are added as their positions become clear. The agreement in the fitting of the molecular model to the observed x-ray diffraction data is measured by a residual, R (*20*), which decreases as the agreement between the observed and calculated data improves. For our initial molecular model, the residual at 3 Å resolution was 0.46. Some preliminary refinement was carried out and a preliminary set of coordinates was published with a residual value of 0.33 at 3.0 Å resolution and of 0.35 at 2.7 Å resolution (*13*). With continued refinement, the R value is now 0.28 at 3.0 Å resolution for 5823 reflections, and 0.29 at 2.5 Å for 7895 reflections (*21*). As the refinement proceeded, it was observed that many potential hydrogen-bonding atoms moved into positions such that hydrogen bonding was implied. At the present stage in the refinement, 91 intramolecular hydrogen bonds have been identified and they have an average distance of 2.90 Å. Our estimate of the standard deviation in atomic positions is about 0.2 to 0.3 Å. The relative deviation is much lower, of course, in the purines and pyrimidines and in the sugar phosphate backbone because their internal distances are constrained in the refinement program. However, the uncertainties in the positions of the noncovalently bonded groups make it necessary to use a knowledge of the geometry as well as interatomic distances in evaluating interactions such as hydrogen bonding. In a few cases, however, we are uncertain, either because the distance is somewhat long or because the geometry is awkward. We have called these probable hydrogen bonds in the comprehensive listing in Table 1. Some hydrogen-bonding interactions may be revised with further refinement, but we do not anticipate a large number of changes. These newly refined coordinates have allowed us to make a number of additional observations concerning the detailed conformation of the molecule. The three-dimensional form of the entire molecule is shown in Fig. 2. Sections of the 2.5Å electron density map [$2F_o - F_c$ map (*19*)] together with portions of the model in its refined position are shown in Fig. 3. Although these newer coordinates are not included here, they are available from the authors on request and have been deposited in the protein data bank (*22*).

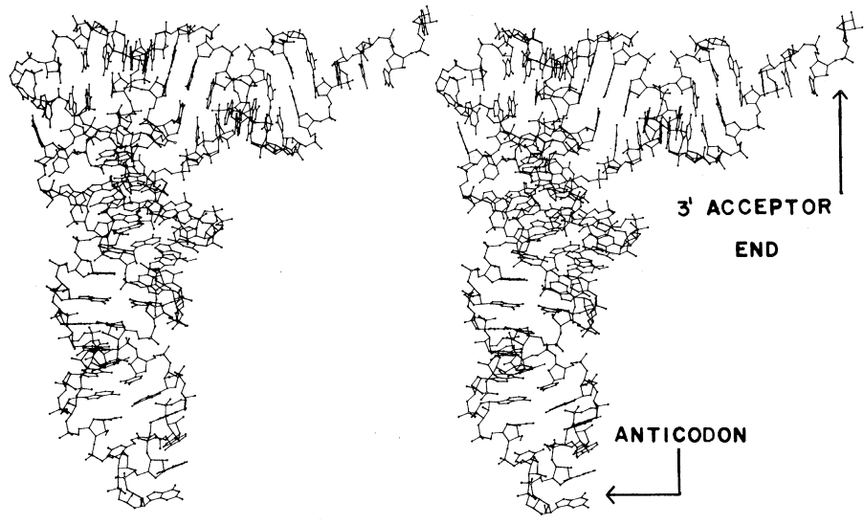

Fig. 2. Stereoscopic diagram of yeast $tRNA^{Phe}$ drawn by using the ORTEP program (*37*). This diagram can be seen in three dimensions by using stereoscopic glasses (*24*). However, the three-dimensionality of the diagram can be seen without glasses if the reader simply lets the eye muscles relax and allows the eyes to diverge slightly, so that the two images are superimposed.

Many Types of Hydrogen Bonding

Figure 1b is a schematic diagram illustrating the folding of the polynucleotide chain in yeast $tRNA^{Phe}$. A coiled tube represents the backbone, and the cross rungs represent the hydrogen-bonding interactions between the bases. As inferred from the cloverleaf diagram, the stem regions are in the form of double helical segments of polynucleotide chain. The black cross rungs in Fig. 1b represent a variety of tertiary base-base hydrogen-bonding interactions, which serve to stabilize the molecule beyond the secondary hydrogen-bonding interactions found in the double helical stem regions. With the exception of the G4 · U69 base pair, all of the base-base hydrogen-bonding interactions in the double helical stems are of the Watson-Crick type (*23*). One of the striking features of the three-dimensional structure of yeast $tRNA^{Phe}$ is the variety of alternative hydrogen-bonding interactions seen in the nonhelical regions; these utilize potentials for hydrogen bonding many of which were hitherto seen only in the structure of synthetic polynucleotides or in the crystal structures of nucleic acid constituents.

An overview of the three-dimensional form of the molecule is seen in the stereoscopic diagram of Fig. 2 (*24*). The structure is dominated by two base-stacking domains, which involve all but 5 of the 76 purine and pyrimidine bases in the molecule. The unstacked bases are in the two variable regions of the D loop (α, D16 and D17; β, G20), in the variable loop (U47), and at the 3′ terminus (A76). Base stacking is the major stabilizing feature of the molecule and is likely to be preserved in the three-dimensional structure of all tRNA molecules (*3*). The horizontal stacking domain contains the acceptor and TψC stems supplemented by two bases from the D loop and all but two of the bases in the TψC loop. The vertical domain includes the two remaining bases from the TψC loop, the D stem supplemented by hydrogen-bonded bases at either end, and the anticodon stem to the anticodon at the bottom of the molecule.

A more detailed view of some of the bases in the molecule is shown in Fig. 3,

which illustrates 11 regions of the electron density map, with the corresponding refined molecular model drawn with heavier lines. Most of the parts of Fig. 3 contain single sections of the electron density map, but some contain other sections 1 Å apart where features with some depth are illustrated. In high-resolution (~ 1 Å) studies of small molecules, an electron density map shows individual atoms as isolated peaks. However, with data at 2.5 Å resolution, the electron density map shows clusters of atoms so that the individual peaks which occur are associated with the bases, the riboses, and the electron-dense phosphate groups, as seen in Fig. 3. In general, bases that are hydrogen bonded are rep-

Table 1. Tertiary hydrogen bonding in yeast phenylalanine tRNA. Standard symbols are used for referring to bases and their atoms: R stands for a purine and Y for a pyrimidine; S is used for the ribose sugar residue, and it is generally followed by an atom designation such as O2′; P stands for the phosphorus atom, and the atoms O1 and O2 are phosphate oxygens. An asterisk indicates probable but not certain hydrogen bonds.

Interaction	Comments	Structural role
	A. Base-base interactions	
1. U8 · A14	Reversed Hoogsteen pairing, explains constant U8 and A14	Stabilizes bend between residues 7 and 8
2. A9 · A23	Poly(rA) pairing of A9 with A23 in major groove of D stem	Stabilizes sharp bend of chain between residues 9 and 10
3. m^2G10 · G45	Single H bond from G45 N2 to m^2G10 O6 in major groove of D stem	Maintains interaction between variable loop and D stem
4. G15 · C48	*Trans* pairing with two H bonds, explains constant R15 and Y48, *trans* pairing required by parallel chain directions	Stabilizes joining of D stem with TψC by stacking; keeps variable loop and D loop together
5. G18 · ψ55	G18 N2 and N3 both within H-bonding distance of ψ55, may partially explain role of constant G18 and ψ55	Maintains interaction of D loop and TψC loop
6. G19 · C56	The only tertiary Watson-Crick base pair partially explains constant G19 and C56	Forms outermost corner of molecule; stabilizes interaction of D and TψC loops
7. G22 · m^7G46	Protonated m^7G46 donates two H bonds to G22 in major groove of D stem	Interaction of extra loop and D stem is also stabilized by electrostatic bond due to charged m^7G46
8. m^2_2G26 · A44	Two H bonds, involve m^2_2G26 N1 and O6 with A44 N1 and N6, propeller twist of bases	Maintains the continuity of stacking interactions from the D stem to the anticodon stem
9. Cm32 · A38	One H bond from A38 N6 to Cm32 O2, may explain constant Y32 in anticodon loop	Stabilizes the anticodon loop
10. T54 · m^1A58	Reversed Hoogsten pairing, partially explains constant T54 and role of constant A58	Maintains stacking in TψC loop
	B. Base-backbone interactions	
1. A9 N6–P23 O2	Type of H bonding found in double helical poly(rA)	Stabilizes sharp bend between residues 9 and 10
2. (a)*C11 N4–S9 O2′	H bond in major groove of D stem, may explain constant Y11-R24 in D stem	Stabilizes sharp bend between residues 9 and 10
or		
(b)*G10 N7–S9 O2′	H bond in major groove of D stem; position 10 is usually a G residue	Stabilizes sharp bend between residues 9 and 10
3. C13 N4–P9 O2	H bond from major groove of D stem to phosphate	Ties residues 8 and 9 to D stem
4. *G18 N2–S58 O1′	One H bond to furanose ring O	Stabilizes interaction of D and TψC loops
5. A21 N1–S8 O2′	A21 N1 faces S8; explains constant A	Stabilizes D loop and folding of chain
6. U33 N3–P36 O2	Explains constant U33	Stabilizes sharp U turn in anticodon loop
7. *A35 N7–S33 O2′	Single H bond to non-Watson-Crick side of central base of anticodon	Stabilizes anticodon conformation
8. *m^7G46–S9 O5′	H bond from variable loop to phosphate 9	Ties residues 8 and 9 to variable loops, helps neutralize positive charge on m^7G46
9. ψ55 N3–P58 O2	Partially explains constant ψ55	Stabilizes sharp U turn of TψC loop
10. G57 N7–S55 O2′	Partially explains constant R57	Stabilizes sharp turn of TψC loop
11. G57 N2–S18 O2′	G57 amino group is near S18	Stabilizes interaction of D and TψC loops by augmenting stacking interaction of G57
12. G57 N2–S19 O1′	G57 amino group is near S19	Stabilizes interaction of D and TψC loops by augmenting stacking interaction of G57
13. C61 N4-P60 O1	Explains constant G53 · C61	Stabilizes TψC loop stacking on TψC stem and positions bases U59 and C60 away from other TψC loop stacking interactions
	C. Backbone-backbone interactions	
1. S7 O2′–P49 O2	Maintains continuity of interrupted ribose phosphate chain	Stabilizes double helical stacking between acceptor and TψC stems
2. *S16 O2′–P18 O2	Holds residue 17 away from molecule	Maintains conformation of α region of molecule
3. *S17 O2′–P19 O2	Holds residue 18 in position to bind to ψ55	Maintains conformation of α region of molecule
4. *S45 O2′–P10 O1	Joins variable loop to sharp bend at residues 9 and 10; likely to supplement interaction B-2a above	Stabilizes juncture of anticodon stem and D stem
5. S46 O2′–P48 O2	Residue 47 bulges out of variable loop; this provides chain continuity between residues 46 and 48	Maintains conformation of central part of variable loop
6. S47 O2′–P50 O1	Joins bulge in variable loop to TψC stem	Stabilizes the bend in polynucleotide chain between residues 48 and 49
7. S48 O2′–S59 O1′	Joins variable loop to TψC loop	Stabilizes stacking between U59 and C48 · G15 base pair
8. S58 O2′–P60 O2	Residues 59 bulges out of TψC loop	Stabilizes stacking of U59 and C60 perpendicular to other bases of TψC loop; also stabilizes m^1A58 stacking on C61

resented by peaks of electron density, which are often separated from each other but sometimes run together at the lower levels of electron density. Figure 3 illustrates nine of the ten total tertiary base-base hydrogen-bonding interactions that are not of the Watson-Crick type. In addition, two sections show other features of interest.

Secondary interactions in tRNA molecules are those involved in the double helical stem regions of the cloverleaf diagram. Interactions involving bases in the nonhelical regions are generally described under the heading of tertiary interactions, and prominent among these are hydrogen bonds. Three types of tertiary hydrogen-bonding interactions are involved in stabilizing the three-dimensional structure of yeast $tRNA^{Phe}$. These include base-base hydrogen bonding, base-backbone hydrogen bonding, and backbone-backbone hydrogen bonding. Table 1 has a list of all the tertiary hydrogen-bonding interactions in these three classes which are observed at the present stage of our refinement analysis of the orthorhombic crystal structure. Several of these hydrogen bonds have been cited earlier (*10–17*). In addition to the interactions of which we are fairly confident, Table 1 includes some interactions which we consider probable but which have a slightly long hydrogen-bonding distance or a somewhat unfavorable geometry. These may be resolved on further refinement. Table 1 also includes comments on the various interactions as well as brief descriptions of their structural roles. Two features are apparent from Table 1. The first is the great diversity of hydrogen-bonding interactions involving the bases. The second is the high frequency with which 2′ hydroxyl groups are involved in hydrogen-bonding interactions, especially in the nonhelical segments of the molecule where the polynucleotide chain has a folded or irregular conformation.

Helical Domains

The most prominent feature in the structure of yeast $tRNA^{Phe}$ is the existence of the double helical stem segments, most of which have a conformation close to the 11-fold type A RNA helix (*25*). In this form of the double helix, the base pairs are tilted approximately 15° from the helix axis and are displaced away from the axis. This creates the effect, visible in Fig. 2, of a very deep major groove in the helical stems and a very shallow minor groove. There is considerable local variation in the helical parameters of the different segments of the molecule, which undoubtedly reflect the local environment. For example, a minor perturbation is found in the acceptor stems associated with the presence of a G · U base pair. This base pair is of the wobble type (*26*). Its electron density is illustrated in Fig. 3j. In this conformation, the G is slightly farther away from the helix axis than it would be in a normal Watson-Crick base pair, while the U residue is slightly closer to it. The electron density map shows a peak of low density in the major groove of the helix, which may be due to an ion occupying that position. The peak of electron density is actually somewhat elongated in the major groove, and this may be the position of one of the spermine molecules in the orthorhombic crystal lattice. Several other counterions and solvent molecules have been visualized in the electron density map and they will be discussed more fully elsewhere.

The helical regions of the acceptor, TψC, and anticodon stems are all fairly close to a conventional RNA-A helix

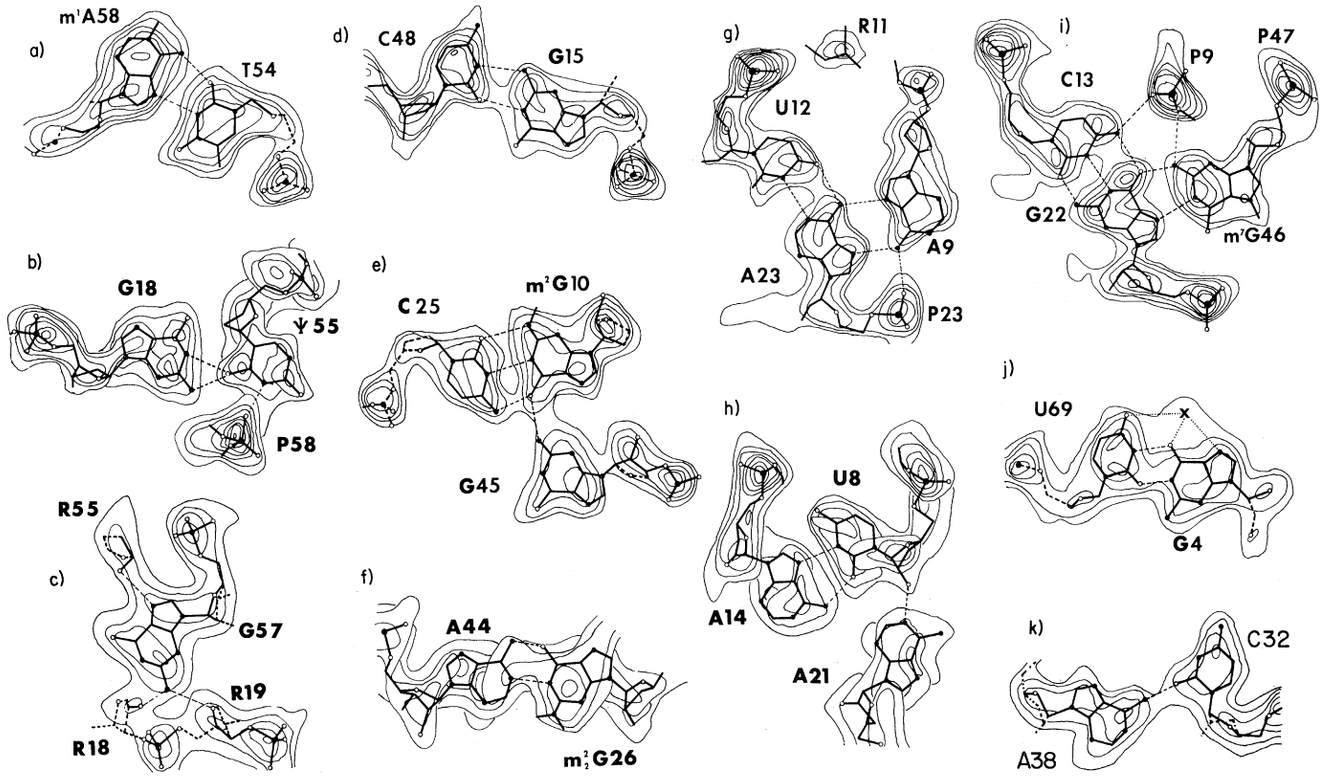

Fig. 3. Electron density sections of the refined model of yeast $tRNA^{Phe}$. Curved lines represent contours of electron density; heavier solid lines represent the molecular model as defined by the refined atomic coordinates. Hydrogen bonds between the bases are shown as thin, dashed lines. Heavier dashed lines are used to show segments of the polynucleotide chain which are outside the plane of the section. Oxygen atoms are shown as small open circles, nitrogen atoms as small solid circles. The phosphorus atoms are slightly larger solid circles. Sections b, f, and h show more than one section, as the segments of the molecule that are illustrated do not all lie in one plane. In these cases, parallel sections 1 Å apart are used. The position marked X in section j corresponds to an ion or solvent molecule which may be coordinating with the bases.

with nearly 11 residues per turn; however, the D helix deviates from this with closer to 10 residues per turn (*27*). This undoubtedly is associated with the large number of interactions which are found in the major groove of this double helix, as discussed below.

The large differences between the RNA double helix and the DNA double helix are due to the steric influence of the 2′ hydroxyl group present in RNA. In tRNA there appear to be a few cases where a hydrogen bond is possible between the O2′ of one ribose and the O1′ of the next ribose. However, the hydrogen-bonding capacity of the 2′ hydroxyl groups is largely unutilized in the helical regions of $tRNA^{Phe}$.

The Uridine Turn (U Turn)

One of the striking features which has emerged from the refinement analysis is the similarity between two regions of the molecule where the polynucleotide chain turns an abrupt corner. This is immediately clear from Fig. 4, which shows a stereoscopic view of the sharp turns in the anticodon loop and the TψC loop. Three important stabilizing interactions are seen. In both cases, the uracil residues (U33 and ψ55) play a key role in defining the character of the turn; hence we call this the uridine turn or U turn in the polynucleotide chain. As shown in Fig. 4a, the polynucleotide backbone starts with phosphate 33 at the upper left, and the chain passes away from the reader and diagonally down to the lower right. The chain changes direction quite abruptly at phosphate 34, largely through the rotation of the P-O5′ torsion angle, as pointed out previously (*28*). The net effect of this change in the direction of the chain places phosphate 35 directly under the pyrimidine ring of uracil 33, so that these are in van der Waals contact. The turn of the chain is stabilized in this conformation by two hydrogen bonds, one of which goes from N3 of uracil 33 to phosphate 36. The other hydrogen bond, which at the present stage of the analysis is slightly long, is between the O2′ of ribose 33 and the imidazole nitrogen (N7) of adenine 35.

A similar conformation is found at the end of the TψC loop (Fig. 4b), where phosphate 57 is in van der Waals contact with the uracil ring of ψ55 while nitrogen atom N3 of ψ55 forms a hydrogen bond with phosphate 58. At the same time, the 2′ hydroxyl group of ribose 55 forms a hydrogen bond to N7 of guanine 57. It appears that the stabilization for this sharp turn derives from three different interactions: (i) the hydrogen bond between the uracil ring and the phosphate group three residues farther down the chain, (ii) the hydrogen bond between the 2′ hydroxyl group and the imidazole nitrogen of the purine ring, and (iii) the van der Waals contact between the phosphate ion and the π electrons of the uracil ring, which may be stabilized through an ion-induced dipole interaction. In both cases, this phosphate group may be regarded as a capping interaction at the end of the large column of bases which form the two long stacking domains of the molecule described above.

The uridine turn is likely to be a component of all RNA's since most of the key components are invariant. Thus, the uridine residues in both cases (uracil 33 and pseudouracil 55) are constant for tRNA's involved in polypeptide chain elongation. Similarly, in the TψC turn, position 57 is always occupied by a purine residue, so that N7 is a constant feature in that position.

In the case of the anticodon loop, the center base of the anticodon A35 can be occupied by any nucleotide, not just a purine. When position 35 is occupied by a uracil or a cytosine, only very small shifts appear necessary for O2′ of ribose 33 to form a hydrogen bond to the non-Watson-Crick side of either uracil O4 or cytosine N4. If a hydrogen bond is found in the latter case, the amino group of cytosine at N4 would donate its hydrogen for the bond, and the hydroxyl would then accept rather than donate its hydrogen. It should be stressed, however, that the final decision with regard to the hydrogen bonding to the center base of the anticodon from the 2′ hydroxyl of ribose 33 will have to await the results of further refinement studies and a knowledge of other tRNA structures.

We are impressed by the fact that the detailed geometry of these turns is so similar in both the anticodon and TψC loops, even though other features of the loops are different. Within the short stretch of three nucelotides, starting with uridine, the polynucleotide chain undergoes a 180° change in direction. Even though the change in the direction occurs largely through a dihedral rotation within one residue, the stabilization for the turn involves interactions with the nucleotides on either side. It will be of interest to see if uridine turns also occur in other RNA structures.

A somewhat similar turn of the polynucleotide chain occurs between residues 9 and 10, but while the O2′ of ribose 9 may be in a position to hydrogen bond to N4 of C11, the turn is more open than the uridine turn. The only other example of the chain reversing direction is in the D loop, where the change takes place gradually over the whole loop.

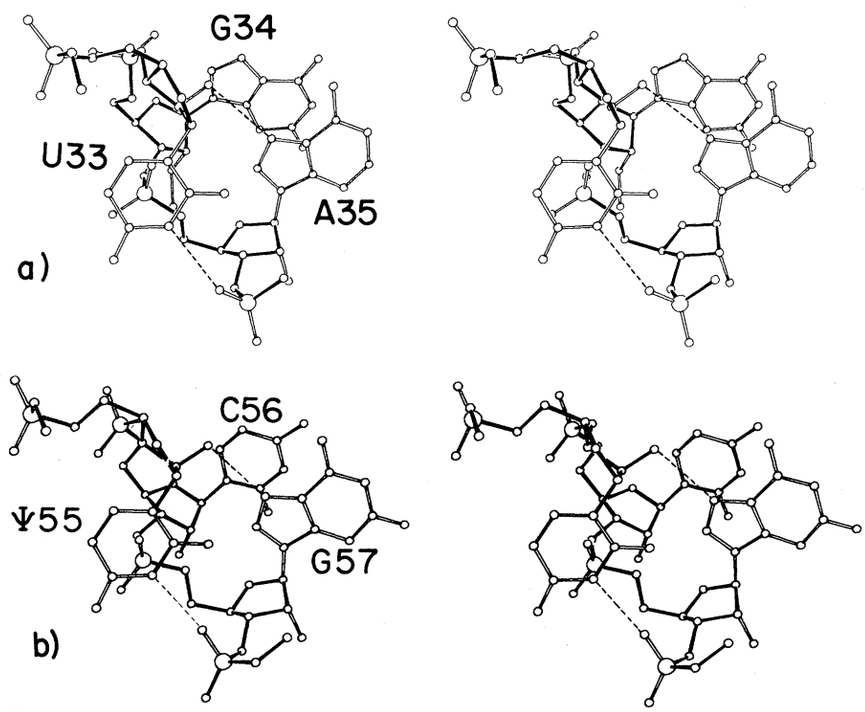

Fig. 4. Stereoscopic views of the uridine or U turn in (a) the anticodon, and (b) the TψC loop. In both cases, the turn is viewed from inside the molecule. It can be seen that phosphate groups lie directly below U33 and ψ55. The turn is stabilized by two hydrogen bonds, which are shown as dashed lines. Phosphorus atoms are drawn as large circles. The ribose phosphate backbone is darkened to clarify the folding of the chain.

The Arch Conformation

One of the interesting features which became apparent on tracing the polynucleotide chain at 3 Å resolution was the fact that the chain bulges in various regions; that is, arches out in such a way as to exclude certain residues from stacking interactions with adjacent nucleotides. In the course of the refinement analyses, we have come to recognize that there appears to be a common structural mechanism for stabilizing these arch domains in which the 2′ hydroxyl group of an adjoining nucleotide plays a crucial role. An example of this can be seen in Fig. 5, which shows a corner of the molecule near the inside of the L, where there is a joining of the acceptor and TψC stems and the variable loop extending down toward the bottom of the diagram. Yeast $tRNA^{Phe}$ has five nucleotides in its variable loop, four of which are involved in base-base hydrogen bonding. One of them, U47, is essentially excluded from the center of the molecule, and that base projects out away from the body of the molecule, where it is readily susceptible to chemical modification (*1*).

The structural mechanism for stabilizing this looping out is seen in Fig. 5. The central feature is the hydrogen bonding of the 2′ hydroxyl group of ribose 46 on one side of residue 47 to the phosphate group of residue 48 on the other side (Table 1, C-5). This has the net effect of pulling together the ribose phosphate backbone in such a way that nucleotide 47 bulges out, projecting its uracil residue away from the rest of the molecule. This conformation is likely to be found in tRNA's that have five nucleotides in the variable loop. It is noteworthy that a substantial number of tRNA's have four residues in the extra loop. As suggested earlier (*3*), this may be brought about by the exclusion of residue 47, with joining of the ribose phosphate chain between positions 46 and 48. This joining could easily be facilitated by small rotations of the ribose and phosphate residues in 46 and 48 without substantial distortion of the remainder of the polynucleotide chain.

There are several examples of arches somewhat similar to that seen in residue U47. Another example is found in the TψC loop, where two of the bases, U59 and C60, are oriented so that they do not stack with the remainder of the bases in the TψC loop, but in a direction virtually at right angles to these (Fig. 6). The bases 59 and 60 initiate the long vertical stacking domain (Fig. 2), which extends down to the anticodon of the molecule. This is achieved partially by creating a bulge for residue U59 (Fig. 6), which is expelled from the stacking interactions of the remainder of the TψC loop through formation of a hydrogen bond between O2′ of ribose 58 and phosphate 60 (Table 1, C-8), leaving U59 stacked on the pair C48 · G15.

Two other probable examples of arch domains are found in the α region of the D loop, where dihydrouracil residues are found in positions 16 and 17. Here we find that D17 is projected out away from the rest of the polynucleotide chain through a hydrogen bond between O2′ of ribose 16 and phosphate 18 (Table 1, C-2) in a manner similar to that described above for U47 and U59. It is interesting that a similar hydrogen bond between the O2′ of ribose 17 and phosphate 19 (Table 1, C-3) has the effect of projecting guanine 18 back toward the molecule, where it interacts with the base ψ55. Since the α region of the D loop has one to three nucleotides, it is clear that this arch domain is used to add additional nucleotides without actually having the nucleotides buried in the body of the molecule. This structural feature is correlated with the fact that nucleotides in the α and β regions are characteristically reactive in chemical modification experiments (*1*).

The arch domain is commonly characterized by the use of an altered ribose conformation. Instead of the normal 3′-*endo* conformation, the ribose residue which donated its O2′ hydroxyl for the hydrogen bonding is usually found in the 2′-*endo* conformation, as in riboses 46, 58, and 17.

It is also possible to have larger bulge or arch domains. Figure 5 shows examples of two other types of bulges. The 2′ hydroxyl of ribose 47 forms a hydrogen bond with phosphate 50 (Table 1, C-6) encompassing two nucleotides. In this

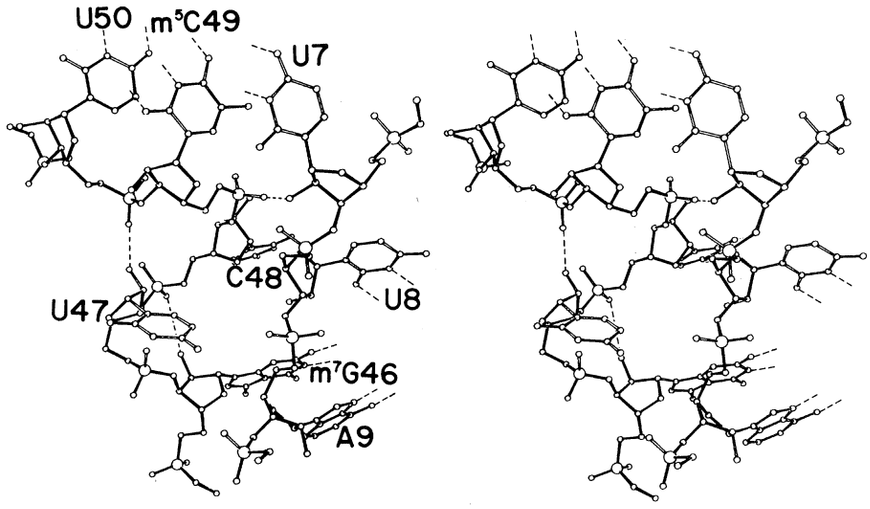

Fig. 5. Stereoscopic view of the juncture between the acceptor and TψC stems and the variable loop near the core of the molecule. This region is near the inside of the L-shaped molecule where it turns the corner. The axis of the acceptor stem and TψC stem is horizontal across the top of the diagram. The molecule is roughly in the same orientation as that shown in Fig. 2 except that the acceptor stem is rotated toward the reader. The coiling of the polynucleotide chain is stabilized by several hydrogen bonds between 2′ hydroxyl groups and phosphate residues, as described in the text. Dashed lines attached to the bases imply that they are hydrogen bonding to other bases, which are not shown.

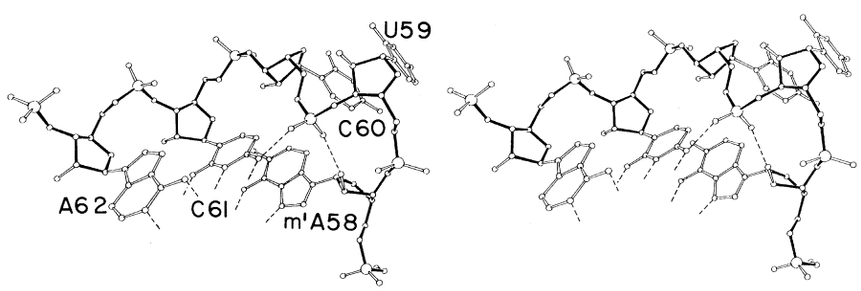

Fig. 6. Coiling of the polynucleotide chain in the TψC loop shown in a stereoscopic diagram. Residues 61 and 62 are part of the TψC stem; m^1A58 is part of the TψC loop. It can be seen that the polynucleotide chain loops out in such a way that residues 59 and 60 do not stack with the rest of the bases. This conformation is stabilized by hydrogen bonding between O2′ of ribose 58 and phosphate 60 as well as between C61 and phosphate 60.

case, the polynucleotide chain has changed direction between residues 50 and 49, which are in the acceptor stem, and residues 48 and 47, which are in the variable loop. This change in the direction of the polynucleotide chain is stabilized by the participation of a 2′ hydroxyl-phosphate hydrogen bond in a manner similar to that seen in the examples above.

A further example of a very large arch or looping out is seen in Fig. 5. Residues 50 and 49 are part of the TψC stem, while residue U7 is part of the acceptor stem. Even though the bases in these two stems are stacked on each other so that they have the appearance of a continuous double helix, the polynucleotide chain is interrupted between residues 7 and 49 with an extremely large bulge which, in fact, constitutes the entire D arm, anticodon arm, and variable loop. This very large arch is similarly stabilized by a hydrogen bond between ribose 7 and phosphate 49 (Table 1, C-1), and ribose 7 is also in the 2′-*endo* conformation. The hydrogen bond uniting ribose 7 and phosphate 49 has the effect of maintaining the continuity of the ribose phosphate chain along one side of the double helix, even though the actual ribose phosphate chain bulges out away from the double helix to form a large segment of the molecule.

In view of the fact that it appears possible to have a very large arching domain, one is tempted to ask whether or not this would be a model of how the large variable loops are integrated into the tRNA structures. Approximately 20 percent of the tRNA sequences have variable loops containing 13 to 21 nucleotides (*1*, *2*). These may be accommodated in much the same way as the single nucleotide bulge of U47, which is shown in Fig. 5. In other words, simply increasing the number of nucleotides in that arch might be a structural basis of the large variable stem and loop structure.

Thus we see that the 2′ hydroxyl group which forms hydrogen bonds to phosphates has the property of stabilizing bulges in the polynucleotide chain which are used in the three-dimensional structure of yeast $tRNA^{Phe}$ in a variety of ways. It is likely that similar arches or looping out of single or multiple residues in which this stabilizing mechanism is used will be found in other RNA structures. Such looping out is commonly seen in the proposed helical stretches of ribosomal and messenger RNA. Indeed, the crucial role of the 2′ hydroxyl group in stabilizing this conformation in the nonhelical regions may be one of the important distinguishing features which separates RNA from DNA. The absence of this stabilizing structure for looping out in DNA may be important in maintaining the fidelity of replication and transcription.

The Corner of the Molecule

A number of additional structural features of interest have emerged in the course of the refinement, and these will be discussed by surveying the molecule from top to bottom in the orientation seen in Fig. 2.

The form of the TψC loop and its interactions with the D loop are likely to be the same in all tRNA's responsible for polypeptide chain elongation because of the large number of invariant nucleotides in this region.

Two features characterize the TψC loop: the sharp bend (U turn) where the polynucleotide chain reverses direction, and the arch structure, which ejects residue U59 from the loop and also makes possible the stacking of pyrimidine C60 outside the loop. The loop is held tightly together by a variety of interactions. One involves the amino group of C61 forming a hydrogen bond to phosphate 60, as shown in Fig. 6 (Table 1, B-13). This is of interest because the base pair C61 · G53 is constant in all tRNA sequences, suggesting that this interaction is important. It appears to be used in stabilizing the turning out of residues 59 and 60 from the remainder of the loop.

The other residues of the loop are characterized by strong stacking interactions at four levels. The first level is the base pair m^1A58 · T54 (Fig. 3a). The importance of stacking interactions in stabilizing these loops is seen in the interesting changes in tRNA of *Thermus thermophilus*, a thermophilic bacteria. Its tRNA's have an elevated melting temperature compared to those of mesophilic organisms (*29*) and systematically have 5-methyl-2-thiouracil instead of thymine. Instead of having an NH. . .O hydrogen bond, as in the pair m^1A58 · T54, there is probably an NH. . .S hydrogen bond (*30*). The higher melting temperature is probably due to the fact that substitution of the sulfur atom in the 2 position of T54 places more polarizable electrons at that site, thereby increasing the strength of the stacking interactions. This suggests that one of the major events which initiates the melting of tRNA's may frequently involve disruption of this corner of the molecule.

In the next stacking level the residue ψ55 of the TψC loop is found hydrogen bonded to G18 of the D loop (Fig. 3b). The O2 atom of ψ55 is within hydrogen bonding distance of both N1 and N2 of G18. Although these distances are not identical, the O2 of ψ55 may be bonding to one or both of these G18 nitrogen atoms. In addition, N3 of ψ55 is hydrogen bonding to phosphate 58 (Figs. 3b and 4b), where it is one of the stabilizing interactions of the uridine turn of that loop.

The electron density of a section through G57 (Fig. 3c) shows that it is stabilized by three hydrogen bonds, one of which involves the 2′ hydroxyl of ribose 55 bonded to N7 of G57. As mentioned previously, this is in accord with the fact that position 57 always contains adenine or guanine. In addition, a purine in position 57 maximizes the stacking overlap in its intercalation between the constant guanines 18 and 19 of the D loop, thereby stabilizing the joining of the two loops. The N2 amino group of G57 is hydrogen bonding to O1′ of ribose 19 and O2′ of ribose 18. These two hydrogen bonds are able to form because the polynucleotide chain of the D loop is fully extended between residues 18 and 19 where they surround the intercalated G57. This elongation is associated with the 2′-*endo* conformation in both ribose 18 and ribose 19. However, when an adenine is present in position 57 in other tRNA's, these two hydrogen bonds would not be formed. In this context it would be interesting to ask whether the tRNA's with adenine residues in position 57 have, in general, a somewhat lower melting temperature than those with guanine there. In view of the fact that thermally stable tRNA's are produced by stabilizing interactions in the TψC loop, this is a possibility.

The outermost corner of the molecule (Fig. 2) is formed by a slightly distorted Watson-Crick pairing between guanine 19 and cytosine 56. This distortion may be related to the extended conformation of residue 19.

The work of Erdmann and colleagues (*31*) has suggested that the TψC loop opens up in the ribosome where it may interact with the 5*S* RNA. From this point of view, it would be interesting to know whether there are instabilities in the structure which suggest that the conformation of this corner of the molecule is less stable than other regions. It is difficult to make a clear assessment of instability from the knowledge of the structure itself. The detailed fitting together of the elements of the D loop with the TψC loop suggests that loop disengagement might be followed by a spontaneous opening of the TψC loop. This question could be subjected to an experi-

mental analysis. If one isolates the 3′ half of the tRNA molecule, it includes the entire TψC stem and loop, but not the D loop. Does the half-molecule still maintain the uridine turn, as illustrated in Fig. 4b? It should be possible to carry out a spectroscopic analysis which would answer this question, and which might shed light on the detailed mechanism of the participation of the TψC loop in protein synthesis.

The Complex Core Region

There is one region in the center of the tRNA molecule where four polynucleotide chain segments interact; we have called this the core region. It includes the four base pairs of the D stem together with residues 14 and 15 of the D loop; residues 8 and 9, which span these bases; and the nucleotides of the extra loop which interact with the D stem. In many ways, this is the most complex portion of the molecule, in that a large number of intricate interactions from these four different chain segments contribute to the total organization of the molecule. The interactions in this area include not only base-base interactions, but also base-backbone and backbone-backbone interactions, as listed in Table 1. Several sections of Fig. 3 illustrate interactions in the core region. At the very top of the core region (using the orientation of Fig. 1b) there is a *trans* Watson-Crick pairing between C48 and G15 (Fig. 3d). Immediately below this is a reverse Hoogsteen interaction between U8 and A14 (Fig. 3h). The constant nucleotide A21 is in the same plane and is in contact with ribose 8 through a hydrogen bond from the ribose 2′ hydroxyl group to N1 of A21 (Table 1, B-5). The next lower level is a complex interaction of all four chains, as seen in Fig. 3i, in which the paired bases of the D stem (C13 · G22) are forming hydrogen bonds in their major groove with m^7G46 and phosphate 9. In addition, a probable hydrogen bond is found between the amino group of m^7G46 and phosphate 9. Since m^7G46 has a positive charge, it is likely that the charge neutralization by phosphate 9 adds to the stabilization, as is suggested in chemical modification experiments (*32*).

Figure 3g shows the interactions of adenine 9 in the major groove of the U12 · A23 base pair of the D stem. Adenine 9 interacts with A23 in a manner similar to that found in the poly(rA) double helix (*33*), including the hydrogen bond between the amino group of A9 and phosphate 23. In the level immediately below in the D stem is a pairing of cytosine 11 with guanine 24. As has been pointed out earlier (*12*), the O2′ of ribose 9 can hydrogen bond to the N4 of C11 (Table 1, B-2b) even though the hydrogen bond is slightly long. This bonding also facilitates a hydrogen bond between the ribose 45 O2′ hydroxyl group and phosphate of G10 (Table 1, C-4). However, O2′ of ribose 9 is also in a reasonable position for forming a hydrogen bond to the imidazole N7 of G10 (Table 1, B-2a). Further refinement will have to be carried out before we can say with certainty which of these two interactions is likely to be found in this molecule. Either conformation would assist in stabilizing the turn in the polynucleotide chain between residues 9 and 10.

The bottom base pair of the core region includes the single hydrogen-bonding interaction of G45 with m^2G10 of the D stem (Fig. 3e). In this position G45 is not in the same plane as the base pair of the D stem to which it is hydrogen bonded, but is stacked on the adjacent A44.

One of the striking characteristics of the core region is the extent to which there is a high density of interactions connecting different parts of the molecule. These interactions include not only the close packing due to size and shape and the stacking of the bases, but also the large number of hydrogen bonds, which provide a great deal of the specificity to the packing. The core region contains 25 percent of the nucleotides in yeast $tRNA^{Phe}$, yet it has almost 50 percent of the tertiary hydrogen bonds listed in Table 1. Many of the interactions in the core region involve invariant or semi-invariant nucleotides, so it is likely that all tRNA molecules have certain common features in the core region. However, as discussed earlier (*3*), tRNA's with a different sequence are likely to have a number of small variations of the basic arrangements seen in yeast $tRNA^{Phe}$.

One base pair involving A44 and m^2_2G26 (Fig. 3f) connects the core region to the anticodon stem. At an early stage in the refinement analysis, it appeared that residue A44 might be in a *syn* conformation (*13*); however, further analysis showed clearly that it is in the *anti* conformation, as seen in Fig. 3f. Several sections of the electron density map are used in drawing Fig. 3f since there is a marked propeller-like twisting between the bases A44 and m^2_2G26, as first described at 3Å resolution (*10*). This twisting is a necessary consequence of the van der Waals interactions due to the dimethylamino group on the guanine residue, which prevents these two bases from being planar. The net effect of the propeller stacking is that it allows A44 to stack on the first base pair of the anticodon stem, while m^2_2G26 can stack quite heavily on the first pair of the D stem. These two stacking interactions would not be possible if the bases did not have this propeller-like twist; thus, dimethylation of the guanine residue effectively maximizes stacking interactions in this joining region.

The Anticodon and Protein Synthesis

The anticodon stem is a typical RNA-A helix. At the present stage in our refinement, however, we have detected an anomaly in the bottom base pair of the anticodon stem A31 · ψ39. The electron density on the ψ residue does not make clear whether the two atoms involved in hydrogen bonding to the adenine are O4 and N3 or O4 and N1. In the former, more normal pairing, the O2 is in the usual position for Watson-Crick pairing in a *syn* conformation. However, the electron density in the O2 region is weak. In the second pairing, ψ39 is in an *anti* conformation and O2 is no longer projecting toward the adenine but away from it, where the electron density is stronger. Further work on the refinement of this structure will be necessary to resolve the conformation in this region. It is interesting to note that an A · ψ pair frequently occurs at the base of the anticodon stem, and the ψ is found exclusively in position 39 and never in position 31. Furthermore, a U is never found in position 39 (*2*).

Immediately below this base pair is an unusual interaction between A38 and C32, for which the electron density is shown in Fig. 3k. It can be seen that the O2 of C32 is close enough to A38 to form a hydrogen bond even though the geometry is not optimal. This interaction is of interest since position 32 is always occupied by a pyrimidine and both C and U have oxygen atoms in the 2 position. Position 38 does not always have adenine, however, even though it usually has a base which can donate a hydrogen atom. Analysis of other tRNA's will be necessary before it is possible to evaluate the generality of this interaction.

Two views of the anticodon together with the hypermodified purine (Y37 base) on its 3′ side are shown in Fig. 7. Figure 7a is a stereoscopic view as seen from the inside of the molecule. Figure 7b is a diagram viewed from the outside

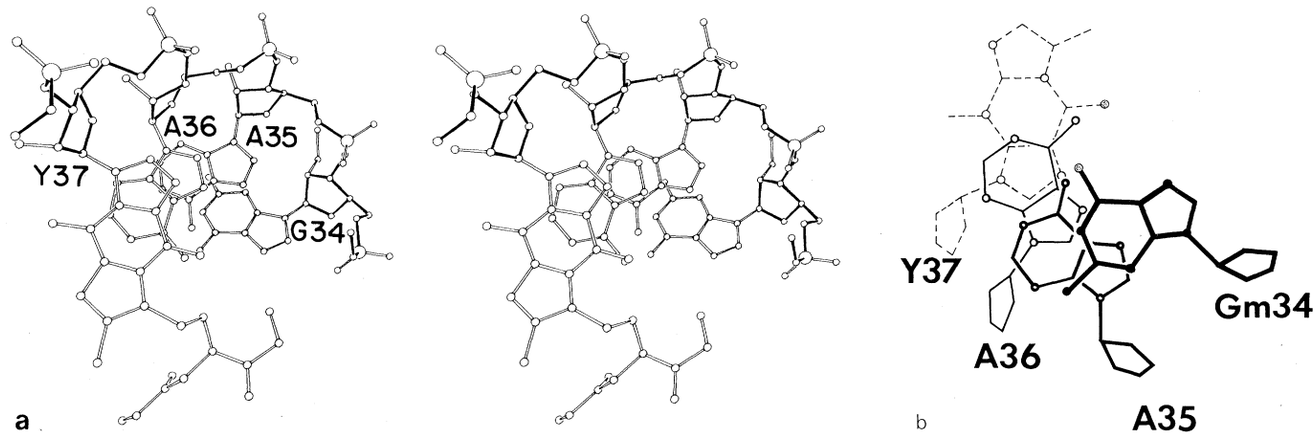

Fig. 7. (a) Stereoscopic view of the anticodon bases 34 to 36 and the hypermodified base Y37 as viewed from the interior of the molecule. It can be seen that the stacking of residues Y37, A36, and A35 is somewhat greater than that of G34 and A35. (b) Diagram illustrating the stacking of anticodon bases 34 to 36 on the hypermodified Y base as viewed from the exterior of the molecule. Oxygen atoms are stippled circles, and nitrogen atoms unstippled circles. Not all of the side chain of the Y base is included. It can be seen that the anticodon takes the form of a right-handed helix.

of the molecule, which shows the three anticodon bases plus the Y base projected onto the plane of A35. From Fig. 7, a and b, it can be seen that residue A36 is well stacked on the Y37 base, and A35 is well stacked on A36. However, G34 is only partially stacked on A35, but this may be due to intermolecular interactions. In the orthorhombic lattice a twofold axis passes near the anticodon such that G34 of one molecule is stacked on G34 of a neighboring molecule. We cannot be certain of the extent to which this affects the detailed stacking of the anticodon.

The significant feature of the anticodon, however, is that the bases are stacked in a right-handed helical array where they are presumably ready to interact with the codon. The anticodon does not have the conformation of one half of a typical RNA-A helix. The helical twist is tighter, having 7 to 8 residues per turn rather than 10 to 11 (*27*). This raises a fundamental question. When the anticodon combines with the codon, does the anticodon loop undergo a conformational change and adopt another conformation—for example, that of an RNA-A helix—or does the codon of the messenger RNA adopt instead the conformation of the anticodon and form a fragment of a tighter double helix with approximately eight residues per turn? We do not know the answer as yet, but it is of interest that when two tRNA molecules with complementary anticodons combine with each other, the anticodon conformation has only a slight change in stacking (*34*).

As discussed above, the turn of the polynucleotide chain at the anticodon is stabilized by the interactions of the uridine turn (Fig. 4a), so that it is entirely possible that the conformation is maintained when bound to the codon. If this is so, then it appears to be impossible for two tRNA's to form codon-anticodon complexes with adjacent codons if the messenger RNA retains the form of an uninterrupted helix, since the adjacent Y base effectively occupies space which the continuation of the codon helix must occupy. However, two adjacent codons could hydrogen bond to two tRNA molecules if there was a disruption in the helical conformation of the messenger RNA in this region. It has been suggested that the messenger RNA might become unstacked between codons while it is being read (*35*). However, we will have to wait for the results of further experiments before questions of this type can be answered.

The anticodon conformation with G34 at the very apex of the molecule leaves that residue in a position where it may be capable of assuming the different conformations required for the wobble pairing (*25*). This possibility for the anticodon conformation was first pointed out by Fuller and Hodgson (*36*).

How could G34 interact in wobble pairing? The wobble interaction implies that the guanine residue could form either a normal Watson-Crick G · C pair, or a G · U pair such as that seen in Fig. 3j. This suggests that two different conformations of the residue G34 may be used, one of which is involved in the normal Watson-Crick interaction and the other in the wobble interaction. The difference in the position of G34 involves a displacement of the base away from the helical axis of approximately 2 Å. We have found that a small conformational change in the region of residue ribose 34 makes possible such a shift in the position of G34.

Summary

In this article, we have described various detailed features of the conformation of yeast $tRNA^{Phe}$ revealed by recent refinement analysis of x-ray diffraction data at 2.5 Å resolution. The gross features of the molecule observed in the unrefined version have been largely confirmed and a number of new features found. The unique role of the ribose 2′ hydroxyl groups in maintaining a series of nonhelical conformations in this RNA molecule has become apparent. Many of these features are a direct consequence of the geometry of the ribose phosphate backbone of RNA molecules, and these may also be found in structured regions of other RNA species as well. Special attention has been directed toward two conformational motifs revealed by this analysis. These include the striking similarity between the TψC and anticodon hairpin turns in the polynucleotide chain, which are stabilized by the participation of uridine in the U turn. In addition, there is frequent occurrence of an arch conformation in the polynucleotide chain which is stabilized by hydrogen bonds from 2′ hydroxyl residues to phosphate groups across the base of the arch. The importance of the 2′ hydroxyl interactions in defining tertiary structure is illustrated by the fact that, in the nonhelical regions, almost half of the ribose residues are involved in O2′ hydrogen-bonding interactions which stabilize the conformation of the molecule.

Two regions which may have considerable functional significance during protein synthesis are described in detail. One involves the joining of the TψC and D loops, which may undergo conformational change in the ribosome during protein synthesis. The other region is the anticodon, which seems conformationally poised, ready to interact with a single-stranded polynucleotide messenger RNA. Analysis of this end of the molecule suggests ways in which the anticodon may interact with the message, although as yet not enough is known to understand how two tRNA molecules interact with adjoining codons on the message. The next goal in this research effort is clearly that of trying to relate the detailed structural conformation of tRNA molecules to their important biological functions in the transmission of genetic information during protein synthesis.

References and Notes

1. For a recent review of tRNA sequences, chemical modifications, and solution chemistry, see A. Rich and U. L. Rajbhandary, *Annu. Rev. Biochem.* **45**, 805 (1976).
2. For a convenient compilation, see B. G. Barrell and B. F. C. Clark, *Handbook of Nucleic Acid Sequences* (Joynson-Bruvvers, Oxford, 1974).
3. S. H. Kim, J. L. Sussman, F. L. Suddath, G. J. Quigley, A. McPherson, A. H. J. Wang, N. C. Seeman, A. Rich, *Proc. Natl. Acad. Sci. U.S.A.* **71**, 4970 (1974).
4. R. W. Holley, J. Apgar, G. A. Everett, J. T. Madison, M. Marquisse, S. H. Merrill, J. R. Penwick, A. Zamir, *Science* **147**, 1462 (1965).
5. The notation for the nucleotide bases is as follows: A, adenosine; T, thymidine; C, cytidine; U, uridine; G, guanosine; ψ, pseudouridine; D, dihydrouridine; and Y, highly modified purine. Also, m denotes methyl and poly(rA) is polyriboadenylate.
6. The early crystallization work is reviewed by F. Cramer, *Prog. Nucleic Acid Res. Mol. Biol.* **11**, 391 (1971).
7. S. H. Kim, G. J. Quigley, F. L. Suddath, A. Rich, *Proc. Natl. Acad. Sci. U.S.A.* **68**, 841 (1971).
8. T. Ichikawa and M. Sundaralingam, *Nature (London)* **236**, 174 (1972); A. D. Mirzebekov, D. Rhodes, J. T. Finch, A. Klug, B. F. C. Clark, *ibid.* **237**, 27 (1972); S. H. Kim, G. Quigley, F. L. Suddath, A. McPherson, D. Sneden, J. J. Kim, J. Weinzierl, A. Rich, *J. Mol. Biol.* **75**, 421 (1973).
9. S. H. Kim, G. J. Quigley, F. L. Suddath, A. McPherson, D. Sneden, J. J. Kim, J. Weinzierl, A. Rich, *Science* **179**, 285 (1973).
10. S. H. Kim, F. L. Suddath, G. J. Quigley, A. McPherson, J. L. Sussman, A. Wang, N. C. Seeman, A. Rich, *ibid.* **185**, 435 (1974).
11. J. D. Robertus, J. E. Ladner, J. T. Finch, D. Rhodes, R. S. Brown, B. F. C. Clark, A. Klug, *Nature (London)* **250**, 546 (1974).
12. J. E. Ladner, A. Jack, J. D. Robertus, R. S. Brown, D. Rhodes, B. F. C. Clark, A. Klug, *Proc. Natl. Acad. Sci. U.S.A.* **72**, 4414 (1975).
13. G. J. Quigley, N. C. Seeman, A. H. J. Wang, A. Rich, *Nucleic Acid Res.* **2**, 2329 (1975).
14. J. L. Sussman and S. H. Kim, *Biochem. Biophys. Res. Commun.* **68**, 89 (1976).
15. J. E. Ladner, A. Jack, J. D. Robertus, R. S. Brown, D. Rhodes, B. F. C. Clark, A. Klug, *Nucleic Acid Res.* **2**, 1629 (1975).
16. C. Stout, H. Mizuno, J. Rubin, T. Brennan, S. Rao, M. Sundaralingam, *ibid.* **3**, 1111 (1976).
17. J. L. Sussman and S. H. Kim, *Science* **192**, 848 (1976).
18. R. Diamond, *Acta Crystallogr. Sect. A* **27**, 436 (1971).
19. R. Huber, D. Kukla, W. Bode, P. Schwager, K. Bartels, J. Diesenhofer, W. Steigemann, *J. Mol. Biol.* **89**, 73 (1974).
20. $R = \Sigma \| F_o | - | F_c \| / \Sigma | F_o |$, where F_o and F_c are observed and calculated structure factors.
21. The R values are based on data with an intensity greater than two estimated standard deviations above background.
22. T. F. Koetzle, *Acta Crystallogr. Sect. B* **29**, 1746 (1973).
23. F. H. C. Crick and J. D. Watson, *Proc. R. Soc. London Ser. A* **223**, 80 (1954).
24. Simple stereoscopic viewers may be purchased from Taylor-Merchant Corp., New York, and Hubbard Scientific Co., Northbrook, Ill. A professional metal viewer may be purchased from Abrams Instrument Co., Lansing, Mich.
25. S. Arnott, D. W. L. Hukins, S. D. Dover, *Biochem. Biophys. Res. Commun.* **48**, 1392 (1972).
26. F. H. C. Crick, *J. Mol. Biol.* **19**, 548 (1966).
27. Helix parameters were calculated by N. C. Seeman as described in J. M. Rosenberg, N. C. Seeman, R. O. Day, A. Rich, *Biochem. Biophys. Res. Commun.* **69**, 979 (1976).
28. S. H. Kim and J. L. Sussman, *Nature (London)* **260**, 645 (1976).
29. K. Watanabe, T. Oshima, M. Saneyoshi, S. Nishimura, *FEBS Lett.* **43**, 59 (1974).
30. U. Thewalt and C. E. Bugg, *J. Am. Chem. Soc.* **94**, 8892 (1972).
31. V. A. Erdman, M. Sprinzl, O. Pongs, *Biochem. Biophys. Res. Commun.* **54**, 942 (1973); D. Richter, V. A. Erdmann, M. Sprinzl, *Proc. Natl. Acad. Sci. U.S.A.* **71**, 3326 (1974).
32. W. Wintermeyer and H. G. Zachau, *FEBS Lett.* **58**, 306 (1975).
33. A. Rich, D. R. Davies, F. H. C. Crick, J. D. Watson, *J. Mol. Biol.* **3**, 71 (1961).
34. H. Grosjean, D. G. Soll, D. M. Crothers, *ibid.* **103**, 499 (1976).
35. A. Rich, in *Ribosome*, M. Nomura, A. Tissieries, P. Lengyel, Eds. (Cold Spring Harbor Laboratory, New York, 1974), p. 171.
36. W. Fuller and A. Hodgson, *Nature (London)* **215**, 817 (1967).
37. C. K. Johnson, *ORTEP* (Report ORNL-3794, Oak Ridge National Laboratory, Oak Ridge, Tenn., 1965).

38. We thank A. H. J. Wang, M. Teeter, and N. C. Seeman for helpful discussions and P. Bellin for expert technical assistance. This research was supported by grants from the National Institutes of Health, the National Science Foundation, the National Aeronautics and Space Administration, and the American Cancer Society.

Early History of Science in Spanish America

Marcel Roche

There is widespread belief that science and technology have been minimal activities in the culture of Latin America. This belief, popular among Latin Americans themselves, finds expression in the words of a North American expert on the region: "To refute the charge that Latin American science has little historical importance, some historians exhume numbers of minor figures whose names are known only to God and to local historians" (*1*). On the other hand, some feel that the history of Latin American science is extensive and that "when fully known should alter the world's view of scientific developments in Spanish and Portuguese America" (*2*). Both views are somewhat extreme, and they make it evident that more studies about Latin American science are needed (*3, 4*).

In this article I attempt only a brief overall view of the main features of science—and technology—in early Spanish America, before the end of the wars of independence in the 1820's, to the exclusion of indigenous lore and of science done locally by non-Spaniards (such as Humboldt or Darwin) with no social or cultural ties with the countries of the region.

General Characteristics

Early Spanish American science has shown two peaks: the first in the 16th century, when the quality of knowledge generated in the region—especially in Mexico—was of a high level, and widely influential in Europe (*5*). The other period of some interest for Spanish American science was the second half of the 18th century, particularly under the reign of Carlos III of Spain (1759 to 1788), when the great expeditions were undertaken, ideas began to circulate, and some local development took place, especially in Mexico and Colombia.

At first sight, science in the region appears to be discontinuous, inasmuch as the main characters seem to have no masters and no followers; but this impression probably would not bear close scrutiny, since science never rises from a vacuum. Further studies may indeed

The author is senior investigator in the Instituto Venezolano de Investigaciones Científicas, Departamento de Estudio de la Ciencia, Apartado 1827, Caracas, Venezuela. The research leading to this article was done in part during a 1-year tenure as Simón Bolívar professor of Latin American studies at the University of Cambridge, Cambridge, England.